ADVANCED MATERIALS
www.advmat.de

Ultralow Dispersion Multicomponent Thin-Film Chalcogenide Glass for Broadband Gradient-Index Optics

Myungkoo Kang, Andrew M. Swisher, Alexej V. Pogrebnyakov, Liu Liu, Andrew Kirk, Stephen Aiken, Laura Sisken, Charmayne Lonergan, Justin Cook, Teodor Malendevych, Fedor Kompan, Ivan Divliansky, Leonid B. Glebov, Martin C. Richardson, Clara Rivero-Baleine, Carlo G. Pantano, Theresa S. Mayer, and Kathleen Richardson**

A novel photothermal process to spatially modulate the concentration of sub-wavelength, high-index nanocrystals in a multicomponent Ge-As-Pb-Se chalcogenide glass thin film resulting in an optically functional infrared grating is demonstrated. The process results in the formation of an optical nanocomposite possessing ultralow dispersion over unprecedented bandwidth. The spatially tailored index and dispersion modification enables creation of arbitrary refractive index gradients. Sub-bandgap laser exposure generates a Pb-rich amorphous phase transforming on heat treatment to high-index crystal phases. Spatially varying nanocrystal density is controlled by laser dose and is correlated to index change, yielding local index modification to ≈+0.1 in the mid-infrared.

Gradient refractive index (GRIN) optics present unique opportunities for control of the chromatic properties of an optical system.[1–5] Novel GRIN materials can be engineered to provide dispersive properties which lie far outside those found in nature, providing new degrees of freedom for optical design[1,2,6–14] as well as the potential for use in new applications.[15–21] In this paper, a novel photothermal process is utilized to spatially modulate high-index nanocrystals within a metastable chalcogenide glass thin film, composed of Ge-As-Pb-Se (GAP-Se) constituents, thereby achieving ultralow dispersion over an unprecedented bandwidth of 1–12 μm wavelength and enabling creation of an arbitrary index gradient required for GRIN optics. Spatially tailorable refractive index change is induced using a two-step fabrication approach, capable of realizing achromatic optical components. Sub-bandgap laser exposure is used to generate Pb-rich amorphous phases within the film, which are then subsequently crystallized into a high-index crystal phase by thermal treatment. The nanocrystal density is modulated by the laser dose, providing a spatially tailorable index change up to ≈+0.1 with high spatial resolution. The measured chromatic properties after the index change were found to be superior to conventional homogeneous infrared media throughout the entire extent of the bandwidth. Knowledge of the material modification mechanism was then extended to form and characterize an optically functional, index-graded component, in the form of a diffraction grating.

Microlens arrays and related planar photonic components have become increasingly important for a wide range of applications, such as compact imaging,[22,23] optical sensing,[24] fiber coupling,[25] and thermo-photovoltaic energy conversion.[26] As a result, there has been growing demand for the development of low-cost, scalable fabrication techniques capable of manufacturing such high performance components. Although significant progress has been made using conventional spherical lenses, chromatic aberration and small operational bandwidth remains a lingering problem for infrared imaging.[1,3,27] These challenges are difficult to overcome due to the lack of materials capable of broadband transmission as well as the feasibility for manufacturing multielement/multimaterial system with microscale dimensions. Gradient index optics (GRIN) presents an interesting solution for chromatic aberration. When an index gradient is induced along the radial axis of an optical element, light is refracted within the volume of the component, unlike conventional homogeneous media where light is only refracted

Dr. M. Kang,[+] A. M. Swisher, Dr. A. V. Pogrebnyakov, Dr. L. Liu, Prof. T. S. Mayer
Department of Electrical Engineering
Pennsylvania State University
University Park, PA 16802, USA
E-mail: tsmayer@vt.edu
A. Kirk, S. Aiken, Dr. C. Rivero-Baleine
Missiles and Fire Control
Lockheed Martin Corporation
Orlando, FL 32819, USA
Dr. L. Sisken, Dr. C. Lonergan, J. Cook, T. Malendevych, F. Kompan, Dr. I. Divliansky, Prof. L. B. Glebov, Prof. M. C. Richardson, Prof. K. Richardson
CREOL
College of Optics and Photonics
University of Central Florida
Orlando, FL 32816, USA
E-mail: kcr@creol.ucf.edu
Prof. C. G. Pantano
Department of Materials Science and Engineering
Pennsylvania State University
University Park, PA 16802, USA
[+]Present address: CREOL, College of Optics and Photonics, University of Central Florida, Orlando, FL 32816, USA

DOI: 10.1002/adma.201803628

along a curved surface. By taking advantage of the additional degrees of freedom associated with volumetric focusing, it is possible to engineer a material system capable of dispersive properties that lie far outside what is found in nature, such as ultralow dispersion across a broadband spectrum, thereby greatly reducing chromatic aberration.[5,13,14] GRIN materials are media in which the refractive index is varied as a function of spatial position, usually through a variation of material composition.[1–12] This variation can be induced by chemical diffusion (i.e., ion exchange[1,7]), lamination of homogeneous, dissimilar materials (as in the case of polymers[8–10] or glasses[11]), and ion implantation[12] to yield either radial or axial GRIN, respectively. Recently, a micropoling method has been shown to enable both lateral and axial refractive index modification with exceptional long-term stability within a near surface (<10 μm) layer in a bulk multicomponent chalcogenide glass.[28] However, these methods typically require substantially complex multistep processes, often lack index gradients with nanoscale resolution, are not compatible with planar geometries or generate optical loss associated with ion beam-induced damage. For the first time, we have demonstrated a novel photothermal process capable of manufacturing a broadband chalcogenide glass with the capability to produce refractive (microlens array) or diffractive (grating) optical structures.

Several high index chalcogenide compositions have received significant interest for applications in infrared optics due to their potential as an affordable material for high transmission over a wide range of wavelengths from 1 to 12 μm.[29–35] Furthermore, chalcogenide glasses have the ability to modulate their refractive index through the formation of high index nanocrystals within the low index glassy matrix.[15,36–45] Here, we exploit these attributes in vapor deposited metastable thin-film GAP-Se glasses that can be transformed to induce high index Pb-rich nanocrystals within the low index glassy matrix. Glass composites with nanocrystals that are sufficiently smaller than the wavelength of light (i.e., less than $\lambda/10$) can be optically described by the parallel effective medium theory; in this case, the effective refractive index of the nanocomposite film increases proportionally to the volume filling fraction of the high-index nanocrystals.[46] Previous work has shown that Pb-rich nanocrystals can be nucleated and grown using homogeneous thermal treatment[36–42] and the attractive properties realized at the lab-scale are retained upon scale-up to commercial sized melts.[42] Although capable of inducing index changes across large areas, temperature gradients are not effective for the creation of complex index profiles required for GRIN optics. Meanwhile, thin-film chalcogenide glasses have been shown to be highly photosensitive to wavelengths near the band gap, facilitating diffusion of elements within the glassy matrix.[47–51] Our novel fabrication process utilizes this phenomenon to achieve highly controlled nanocrystal growth using a two-step approach (**Figure 1**a). When exposed to a 1064 nm sub-bandgap laser, the GAP-Se film undergoes photodissociation, breaking the bonds between neighboring atoms. The resulting instability

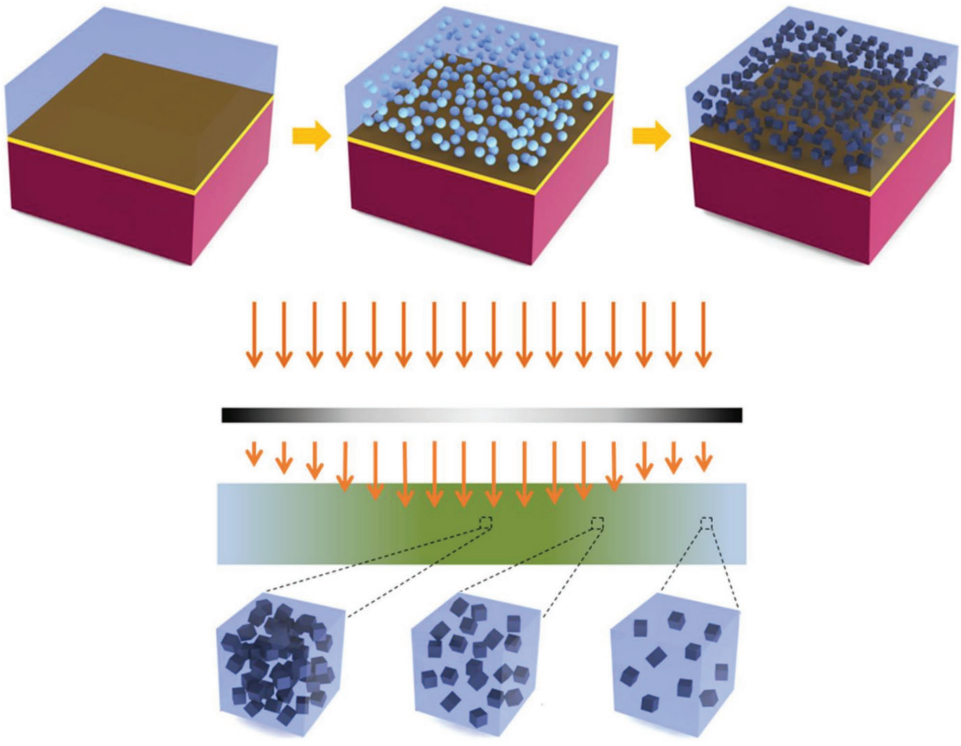

Figure 1. GRIN optics and photothermal manufacturing process on GAP-Se films. (Top) Fabrication process flow for the controlled nanocrystal growth in a GAP-Se film. The film is deposited by coevaporation on an infrared transparent substrate with an antireflective coating at the interface. Laser exposure then induces Pb-rich amorphous phases (blue spheres), which are then converted into high-index nanocrystals (black cubes) by thermal treatment. (Bottom) The concentration of nanocrystals is spatially modulated by varying the exposure dose across the film through the use of a grayscale mask, producing a highly controlled index gradient along the lateral direction.

encourages the formation of a well-dispersed, sub-wavelength size Pb-rich amorphous phase; the concentration of this phase is dependent upon the exposure dose and remains highly localized to the irradiated regions. The laser-induced amorphous phases are then selectively crystallized into a high-index crystal phase using a subsequent thermal treatment of 150–200 °C, modifying the optical properties of the glass. Unlike direct thermal crystallization, the photothermal process can achieve nanoscale patterning resolutions by directly controlling the concentration of the Pb-rich phase. This method provides a potential low-cost manufacturing process for the scalable production of high performance GRIN optics; a grayscale mask can be used to spatially vary the exposure dose across the GAP-Se film to fabricate achromatic microlens arrays (Figure 1b).

The laser exposure-induced phase separation of the otherwise homogeneous amorphous film is the key to the spatially selective crystallization process. By selectively preforming the Pb-rich amorphous phases in the glassy matrix with a laser, the refractive index can be selectively varied across the film, which is essential to designing the final optical profile of the GRIN component. Our novel fabrication approach is demonstrated on GAP-Se films vapor deposited on infrared transparent substrates, using an antireflective coating at the interface to mitigate the effects of standing waves. The film composition was chosen to have a high PbSe concentration (14%$GeSe_2$–42%As_2Se_3–44%PbSe [at %]), to enhance photoinduced phase separation and nanocrystal formation and as a means of tailoring the dispersive properties for optimal chromatic performance. In order to maintain stability, films underwent a low temperature anneal of 120 °C for 4 h to reduce residual stress prior to laser exposure. **Figure 2**a–d shows nanoscale images at varying stages of the photothermal process, including bright field (BF) transmission electron microscopy (TEM) images as well as selected-area electron diffraction (SAED) patterns. The GAP-Se film is initially homogeneous and amorphous, as shown in Figure 2a. When exposed to dose of 7.56×10^3 J cm^{-2} via a 1064 nm laser at room temperature, the film separates into two distinct amorphous phases, a dark Pb-rich phase and a bright Pb-deficient phase (Figure 2b). Subsequently, a 190 °C thermal treatment promotes selective crystallization of the Pb-rich phase, as is indicated by the crystalline fringes of the dark phases in the TEM image and spotted SAED pattern in Figure 2c. Neither modification to the Pb-deficient phase nor the unexposed region of the film occurs under these thermal treatment conditions. The concentration of nanocrystals created can be directly modulated by varying the exposure dose.

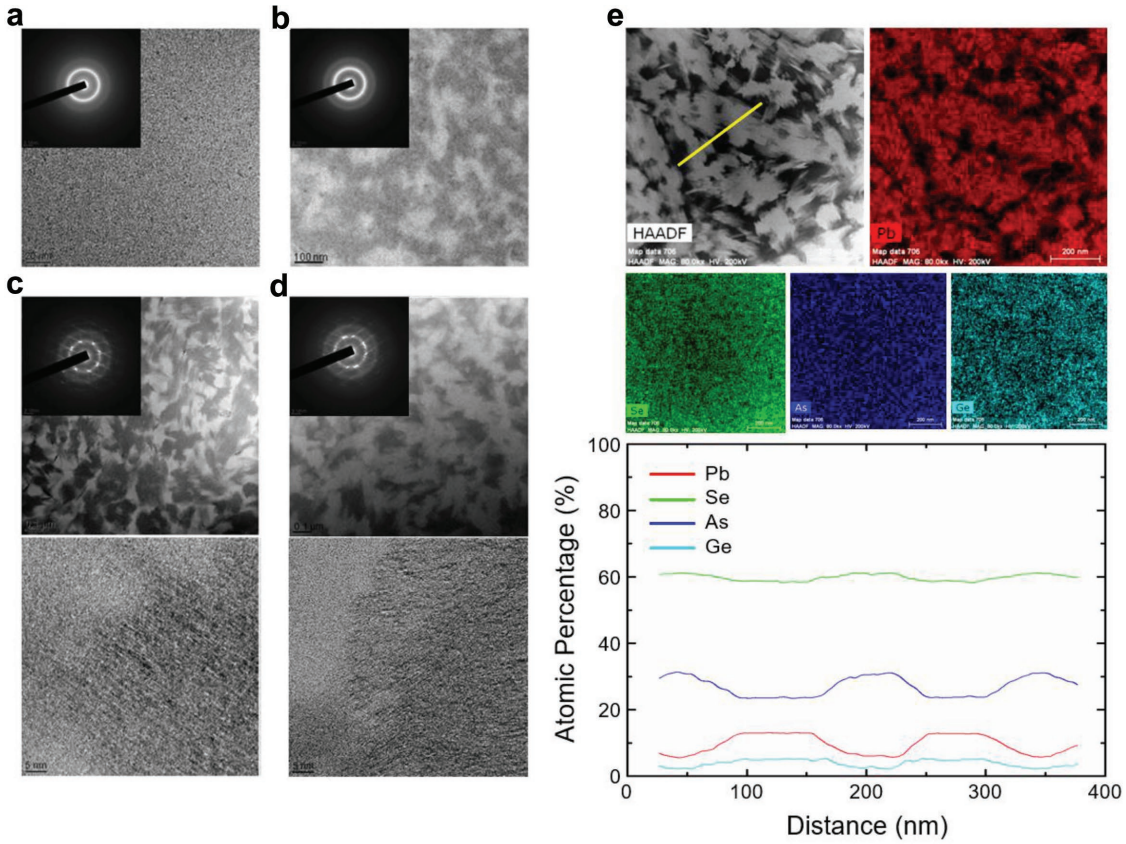

Figure 2. BF TEM images, SAED patterns, and DF TEM images along with XEDS maps (in an STEM mode) of GAP-Se films. a) Unexposed GAP-Se film following stress relieving anneal. The scale bars vary. b) Laser exposed (7.56×10^3 J cm^{-2}) film has a Pb-rich amorphous phase (dark) in the amorphous Pb-deficient glass matrix (bright). c) The Pb-rich phase in sample b is selectively crystallized following a thermal treatment of 190 °C for 30 min. d) GAP-Se film following a laser exposure of 1.01×10^3 J cm^{-2} and a subsequent thermal treatment of 190 °C for 30 min. e) Composition analysis of GAP-Se films following laser exposure and post-thermal treatment where the DF TEM image, XEDS maps (top), and spatial linear composition profiles (bottom) of the constituents indicate the spatial segregation of Pb atoms.

Figure 2d shows a lower density of the nanocrystals in the TEM image and spots in the SAED pattern when the exposure dose is reduced to 1.01×10^3 J cm^{-2}. It is important to note that in the absence of the laser exposure, temperatures greater than 200 °C are required to crystallize this glass, and results in spontaneous nanocrystal growth randomly within the glass matrix. This latter condition is undesirable because the size and distribution of these crystals can vary widely, increasing scattering and reducing transmission. The important point is that the Pb-rich nanocrystals only form in those regions where laser exposure has been carried out to phase separate the material, thereby lowering the activation energy for crystallization to temperatures between 150 and 200 °C. X-ray energy dispersive spectroscopy (XEDS) was utilized to analyze the laser exposure-induced redistribution of constituents including Pb, Se, As and Ge atoms in the films which was laser exposed at a dose of 7.56×10^3 J cm^{-2} and postannealed for 30 min at 190 °C. A dark field (DF) TEM image was collected and XEDS maps corresponding to all constituents in a scanning transmission electron microscopy (STEM) mode were generated. Spatial linear composition profiles of the constituents in the XEDS maps are shown in Figure 2e. The distribution of Pb in the XEDS map can be clearly correlated with that of the bright phase in the DF TEM image, suggesting that Pb atoms are segregated into the bright phases in the DF TEM image upon laser exposure. The atomic percentages of the four constituents were then quantified over a spatial region that spanned several bright and dark phase regions in the DF TEM image where it is clear that the nanocomposite consists of Pb-rich and Pb-deficient regions. Meanwhile, the spatial distribution of As atoms is opposite to that of Pb atoms while the distributions of Se and Ge remain relatively uniform across the region studied. The sub-wavelength segregation of Pb has a particular importance since Pb-containing crystalline phases such as PbSe and $Ge_{0.1}Pb_{0.9}Se_{1.0}$ have been found to be formed via X-ray diffraction. The refractive indices of these crystalline phases [PbSe and $Ge_{0.1}Pb_{0.9}Se_{1.0}$, respectively] are greater than those of crystalline As_2Se_3[40,41] and Se[40,41] as well as their amorphous counterparts (i.e., amorphous bulk GAP-Se glasses)[40,41] and therefore play the dominant role in increasing the effective refractive index, n_{eff}, of the transparent optical nanocomposite.

Multicomponent melt-quenched bulk chalcogenide glasses can exhibit metastable or unstable phase separation, limiting their use in optical applications.[52–55] Films formed from these glasses often do not exhibit such morphology as the thermal history imparted in deposition is vastly different and the as-deposited metastable structure now further from equilibrium can remain amorphous. The photosensitivity of the as-deposited amorphous chalcogenide thin-film glasses enables their chemical bonds to reconfigure under laser exposure with a wavelength near the band edge.[47–51] Specifically, the lone-pair electrons with states located at the top of the valence band of the chalcogenide atoms play a dominant role in the thin-film glass' photosensitivity. When sub-bandgap light excites the non-bonding electrons to a sub-band energy state, electron–hole pairs are created. The electron–hole pairs change the valence of neighboring atoms and their chemical bonds, thereby contributing to the thermodynamically driven phase separation process. Electronic excitation of network bonds by the photoionization process increases the local density of nonbonded atoms in the laser-exposed volume so that the system can respond to the instability of the thin-film glass through macroscopic physical property changes, such as the Pb-rich phase separation. This effect is particularly favorable in vapor-deposited thin films since they are far from equilibrium,[56] i.e., when the source materials are deposited on a room temperature or cold substrate, they condense into an amorphous film with a high concentration of atomic/molecular clusters with strained bonds, thereby lowering the activation energy required to transform them to a more stable configuration. Thus, 1064 nm laser exposure is able to provide the activation energy required to drive the phase separation described above. The Pb-rich amorphous phase is itself unstable against crystallization and so heating to temperatures of 150–170 °C is sufficient to crystallize the Pb-rich phase. It is important to note that in the absence of the laser exposure, temperatures greater than 200 °C are required to crystallize this glass. Therefore, the Pb-rich nanocrystals only form in those regions where laser exposure has been carried out to phase separate the material, thereby lowering the activation energy for crystallization.

To design GRIN optical elements, it is essential to correlate the morphological changes during the photothermal process to the corresponding changes in the postheat treated film's optical properties. Through understanding of both the laser exposure and the thermal treatment mechanisms in our films, the amorphous Pb-rich phase formation and the crystallization process can be engineered to spatially modify the optical properties of the film. **Figure 3**a shows spectroscopic ellipsometry (SE) measurements of the effective refractive index for an experimental group of films which have been laser exposed with a dose of 7.56×10^3 J cm^{-2} and subsequently annealed for 30 min at temperatures varying between 150 and 200 °C. Irradiated films which were not heated above 150 °C remained fully amorphous and were not found to produce a measurable index change, indicating that the nanocomposite comprised of multiple amorphous phases has an equivalent refractive index to the initial homogeneous film, despite structural differences. As the thermal treatment temperature is increased from 150 to 200 °C, the volume fraction of the Pb-rich amorphous phases that are converted into high index nanocrystals increases, leading to a corresponding change in the effective index consistent with the microstructural evolution observed in Figure 2. However, films which have not undergone laser exposure fail to change in index until 230 °C, when sudden uncontrolled nanocrystal growth occurs spontaneously within the entirety of the glassy matrix. The Pb-rich amorphous phases, being more unstable than the homogeneous film, require lower activation energy to induce crystallization. By taking advantage of this transition region between the regimes, the photothermal process can be utilized to induce index change in selective regions of the film that a strictly thermal process cannot achieve. To determine the influence of laser exposure on the GAP-Se films, an exposure matrix with a wide range of doses varying from 5.05×10^2 to 1.51×10^4 J cm^{-2} and intensities from 1.05×10^1 to 1.51×10^4 kW cm^{-2} was selected for further investigation. Figure 3b shows SE measurements of the effective index changes at a wavelength of 4 μm following a thermal treatment of 30 min at 190 °C. The optical properties of the GAP-Se film

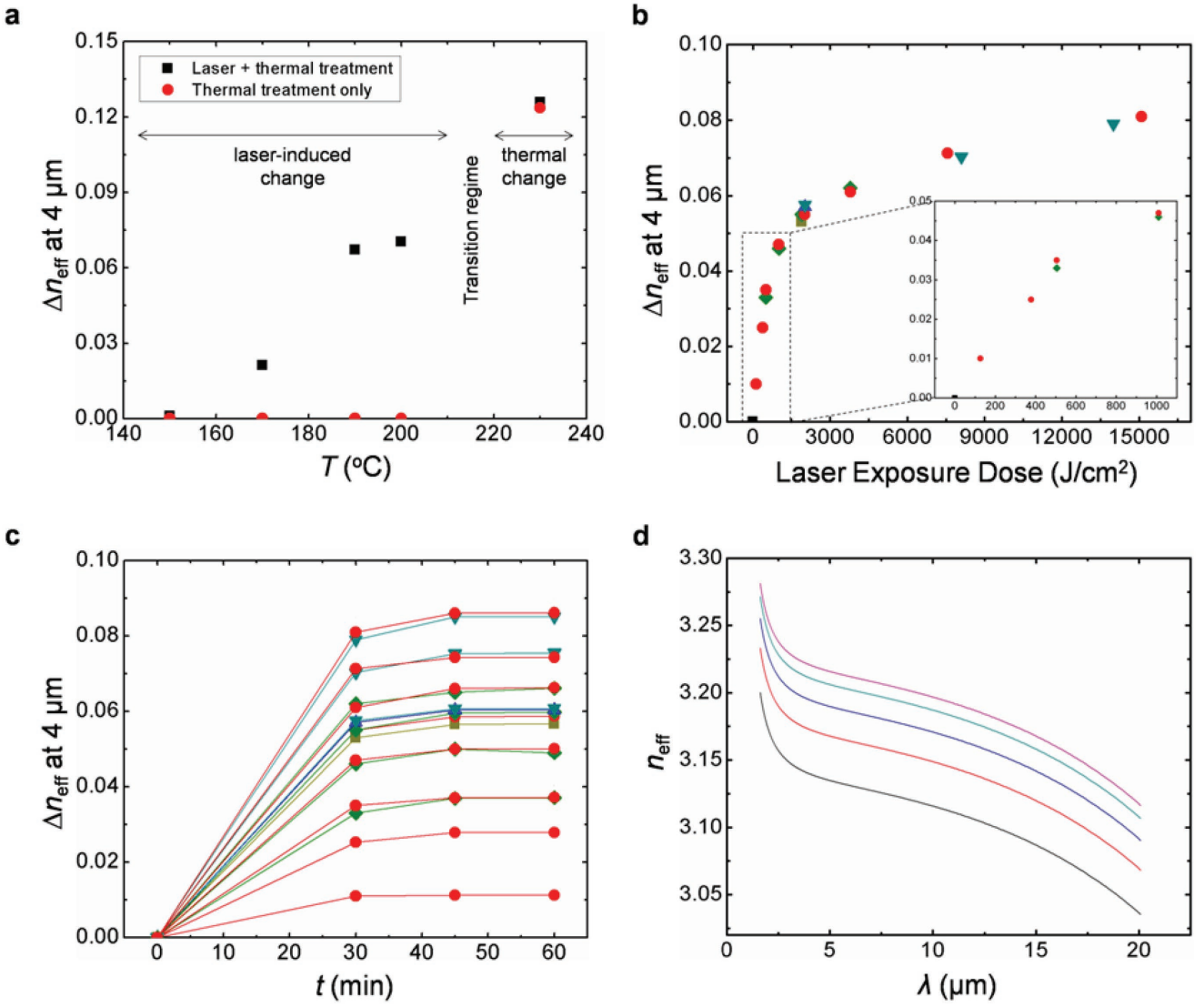

Figure 3. n_{eff} of GAP-Se films as functions of various laser exposure and thermal treatment conditions. a) Index change at 4 μm versus thermal treatment temperature (T) for films which underwent the photothermal process and thermal treatment alone. b) Index change at 4 μm is dependent upon laser exposure dose. c) Δn_{eff} at 4 μm versus post-thermal treatment time (t) for films which were laser-exposed with the doses used in (a). For both (b) and (c), a range of laser exposure irradiances (■: no exposure, ■: 1.05×10^1 kW cm^{-2}, ◆: 2.10×10^1 kW cm^{-2}, ●: 4.20×10^1 kW cm^{-2}, ▲: 8.40×10^1 kW cm^{-2}, ▼: 2.92×10^2 kW cm^{-2}) were used. d) Index change versus wavelength (λ) of films which underwent laser exposures with a range of doses (——: no exposure, ——: 5.05×10^2 J cm^{-2}, ——: 2.02×10^3 J cm^{-2}, ——: 7.56×10^3 J cm^{-2}, ——: 1.51×10^4 J cm^{-2}) and post-thermal treatment for 30 min at 190 °C.

were found to be solely dependent on the exposure dose with the index change having a hyperbolic relationship as a function of fluence allowing for greater control during device manufacturing. By controllably producing index changes via variations in the laser exposure dose, we can achieve a nanoscale patterning resolution that would otherwise not be possible with a thermal gradient or other methodology (i.e., ion exchange or lamination) that relies on diffusion. In order to demonstrate that the effective index change is dependent on exposure dose and not the thermal treatment, we tested the samples at a thermal treatment temperature of 190 °C for varied postexposure anneal times (Figure 3c). The changes in refractive index were found to saturate following a 45 min anneal, demonstrating that the laser-induced amorphous phases are completely crystallized after that duration and that spontaneous crystallization within the surrounding matrix phase does not occur.

The chromatic aberration of an optical system is typically corrected through the creation of an achromatic doublet; this approach uses two lenses with complementary dispersive properties to offset the fluctuations in focal length. However, this approach is not well suited for broadband applications as the dispersive properties of a homogeneous media tend to vary considerably across the 1–12 μm broadband spectrum, causing inconsistent color performance. GRIN optics can overcome this problem by producing unique dispersive properties that cannot be achieved by conventional homogenous spherical lenses. By

Table 1. The calculation of V_{homo} and V_{GRIN} for GAP-Se glasses based upon effective indices of amorphous and crystallized films across SWIR, MWIR, and LWIR spectral bands in Figure 3d.

Sample	Index					
		n_{eff} at SWIR (1.6–3 μm)		n_{eff} at MWIR (3–5 μm)		n_{eff} at LWIR (8–12 μm)
Amorphous	*A*	3.201 at 1.6 μm	*G*	3.150 at 3 μm	*M*	3.125 at 8 μm
	B	3.163 at 2.3 μm	*H*	3.141 at 4 μm	*N*	3.117 at 10 μm
	C	3.150 at 3.0 μm	*I*	3.136 at 5 μm	*O*	3.107 at 12 μm
Crystallized	*D*	3.282 at 1.6 μm	*J*	3.231 at 3 μm	*P*	3.206 at 8 μm
	E	3.244 at 2.3 μm	*K*	3.222 at 4 μm	*Q*	3.198 at 10 μm
	F	3.231 at 3.0 μm	*L*	3.217 at 5 μm	*R*	3.188 at 12 μm
V_{homo} for amorphous	$\frac{B-1}{A-C}=42.4$		$\frac{H-1}{G-I}=152.9$		$\frac{N-1}{M-O}=117.6$	
V_{homo} for crystallized	$\frac{E-1}{D-F}=43.6$		$\frac{K-1}{J-L}=159.7$		$\frac{Q-1}{P-R}=123.8$	
V_{GRIN}	$\frac{E-B}{(D-A)-(F-C)}=-1950$		$\frac{K-H}{(J-G)-(L-I)}=-7712$		$\frac{Q-N}{(P-M)-(R-O)}=-7644$	

introducing an index gradient along the radial axis of the optical element, light can be refracted within the volume as opposed to along a curved surface. As the dispersive properties of the component phases which bring about the volumetric focusing are different than in the case of a homogenous spherical lens, new degrees of freedom are achieved for chromatic aberration correction.[1–6] The 14%$GeSe_2$–42%As_2Se_3–44%PbSe GAP-Se film composition was selectively engineered to modulate the concentration of high-index nanocrystals, thereby providing ultralow dispersion across the entire 1–12 μm broadband spectrum. The Abbé number at a corresponding spectral range for a homogeneous media and a radial GRIN lens be respectively defined as $V_{homo} = (n_{middle} - 1)/(n_{short} - n_{long})$ and $V_{GRIN} = (\Delta n_{middle})/(\Delta n_{short} - \Delta n_{long})$ where n is the refractive index and Δn is the change in refractive index for the material system at the corresponding positions within the chosen spectrum.[11] To determine the chromatic performance of the GAP-Se glass, we tested a series of films exposed to varying doses from 5.05×10^2 to 1.51×10^4 J cm^{-2}, which had been thermally treated for 30 min at 190 °C (Figure 3d). **Table 1** shows the calculation of V_{homo} and V_{GRIN} for GAP-Se glasses based upon effective indices of amorphous (as-stress relieving annealed and no exposure) and crystallized (the highest dose of 1.51×10^4 J cm^{-2} and post-thermal treatment for 30 min at 190 °C) films across short-wave infrared (SWIR), mid-wave infrared (MWIR), and long-wave infrared (LWIR) spectral bands in Figure 3d. While the homogeneous dispersive properties of the GAP-Se film were found to be similar to other conventional broadband materials, the radial GRIN Abbé number was found to be more than an order of magnitude greater and had remarkable consistency across the full bandwidth (**Table 2**). The Abbé number of the radial index gradient was calculated to be –1950, –7712, and –7644 in the SWIR (1.6–3 μm), MWIR (3–5 μm), and LWIR (8–12 μm) regions, respectively. The GRIN properties are also unique in that they have a negative polarity, indicating that higher wavelengths are refracted more sharply than lower wavelengths. While these dispersive properties have been realized for a specific dose and heat treatment protocol, variation in these treatment conditions can be utilized to alter/tune the composite's desired dispersive attributes. These features make our GAP-Se composition an ideal candidate for many broadband applications as it has been shown to provide excellent chromatic performance across the entire spectrum with just a single lens element, which cannot be achieved with conventional spherical optics.

In order to take advantage of the unique dispersive properties associated with volumetric focusing, it is essential to demonstrate the lateral patterning resolution of the GAP-Se film by introducing spatial variations in the exposure dose. An optically opaque binary Au mask with a width of 1 μm and a pitch of 3.5 μm was deposited on top of the GAP-Se film, and laser exposed with a dose of 7.56×10^3 J cm^{-2} (**Figure 4**a). BF TEM images and corresponding SAED patterns were taken from four

Table 2. Abbe numbers for common IR media and GAP-Se glasses (14%$GeSe_2$–42%As_2Se_3–44%PbSe [at%] film) across SWIR, MWIR, and LWIR spectral bands.

Material	Wavelength		
	V_{SWIR} (1.6–3 μm)	V_{MWIR} (3–5 μm)	V_{LWIR} (8–12 μm)
Amorphous material transmitting infrared radiation (AMTIR-1)	41.9	201.9	109.4
BaF_2	84.4	45.2	7.1
CsI	124.3	464.7	238.6
GaAs	30.6	146.7	103.4
Ge	N/A	107.6	770.3
Si	49.2	237.8	N/A
ZnS	74.3	111.8	22.9
ZnSe	62.0	176.9	57.9
GAP-Se: amorphous	42.4	152.9	117.6
GAP-Se: crystallized	43.6	159.7	123.8
GAP-Se: radial GRIN	–1950	–7712	–7644

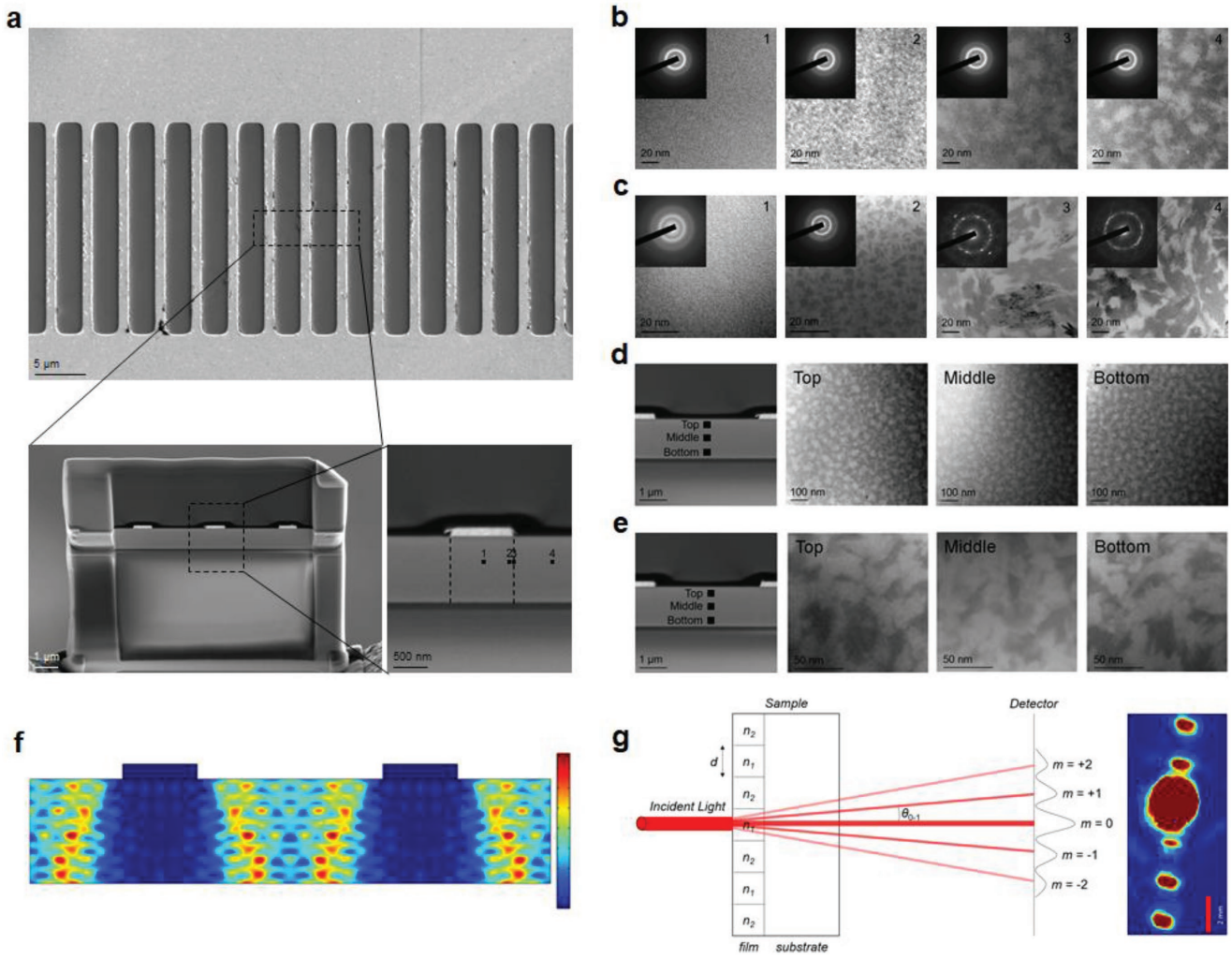

Figure 4. The spatial modulation of laser-induced Pb-rich phases in GAP-Se films and its optical functionality in the form of an infrared diffraction grating. a) (Top) A top view scanning electron microscopy (SEM) image of the GAP-Se film with a binary Au exposure mask, (bottom left) a cross-sectional view SEM image of the layers including the fused silica substrate, 0.143 µm thick $SiO_{0.9}$ AR coating, 1.4 µm thick GAP-Se film, 185 nm thick Au metal pattern, and protective carbon layers, and (bottom right) the enlarged SEM image where regions of interest in the film are specified. b) BF TEM images and SAED patterns corresponding to the regions labeled in the laser exposure cross-section. The amorphous Pb-rich phases evolve in size from 10 to 50 nm between regions 2 and 3, until the film is fully exposed in region 4. c) BF TEM images and SAED patterns of the multiple regions in the postannealed (30 min at 190 °C) film following laser exposure. Region 1 remains amorphous while the Pb-rich phases in regions 2–4 are fully crystallized. d) BF TEM images of top, middle, and bottom regions in the film before thermal treatment. e) DF TEM images of top, middle, and bottom regions in the postannealed film. f) COMSOL full-wave simulation of the laser-exposed sample with metal patterns. The Figure shows $|E^2|$ inside the film under a TE-polarized wave with a wavelength of 1064 nm. Both the AR coating and fused silica substrate are hidden from the image for clarity. g) The diffractive performance of the laser-written and postannealed grating structure measured in transmission at $\lambda = 2$ µm where multiple diffraction spots are clearly observed, confirming an index modulation within the structure.

regions labeled with 1, 2, 3, and 4 to observe both the lateral and in-depth microstructures before (Figure 4b) and after (Figure 4c) thermal treatment for 30 min at 190 °C. As shown in Figure 4b, the GAP-Se film remains homogeneous and amorphous in region 1 directly beneath the Au mask. The Pb-rich amorphous phases gradually transition in size from 10 to 50 nm between regions 2 and 3, until the film is fully exposed in region 4. Following thermal treatment, region 1 still remains homogeneous and amorphous while the Pb-rich phases in regions 2–4 are fully crystallized by the subsequent thermal treatment, as shown in Figure 4c. It is important to note that the concentrations of Pb-rich phases in each of the corresponding regions are consistent before and after thermal treatment, showing no signs of localized diffusion. This demonstrates that our novel photothermal process is capable of controllably introducing arbitrary index gradients with nanoscale resolution via a single shot laser exposure. This also suggests that a grayscale mask can be implemented as a potential low-cost manufacturing process for scalable production of high performance achromatic microlens arrays. It is also important to see whether the size and density of the resulting Pb-rich phase in each region of the film is independent of the depth too. Figure 4d shows BF TEM images of top, middle and bottom regions in the film before thermal treatment where the size and density of the laser exposure-induced amorphous Pb-rich phase appear to be uniform, independent of the depth. Figure 4e shows DF TEM images of those regions in the film after thermal

treatment, and similarly, the distribution of the Pb-rich nanocrystals is uniform along the depth. In parallel, full-wave COMSOL simulations were carried out for the Au mask test structure to model the resulting effective refractive index distribution. Figure 4e shows the electric field magnitude, $|E^2|$, inside the film under the illumination of a transverse electric (TE)-polarized wave with a wavelength of 1064 nm. Both the air above the film and the antireflective coating/fused silica substrate below the film are hidden from the image for clarity. The incident light is partially blocked by the Au metal pattern which leaves shadowed regions in the film. The transition regions near the edges of the metal patterns are clearly shown, and the light intensities in the shadowed and open regions are different by upward of three orders of magnitude. The lateral transition of $|E^2|$ in the film is consistent with our experimental results where the density of laser-induced Pb-rich phases varies in the similar fashion. The excellent agreement between the experimental measurements and computational simulations allows for accurate modeling of complex index gradients within the GAP-Se film. To extend this mechanistic understanding to realize its applicability in an optically functional component, we utilize the photothermal process-induced index modulation in our GAP-Se film, to create a volume grating structure within the film structure. Specifically, the surface of the film was exposed with a laser beam for 6 h at 10 W which went through a mask, thereby creating a 1D volume grating structure consisting of alternating high and low index regions with a target lateral spacing of 23.7 μm. Following exposure, the film was heat treated for 30 min at 190 °C to realize growth of nanocrystallites within the exposed region. This dose + heat treatment protocol was chosen to create a localized target Δn of 0.08, based on use of data from the film's calibrated response shown in Figure 3b. To assess the diffractive properties of the grating, the structure was interrogated in transmission (λ = 2 μm) mode. Under these measurement conditions, diffraction was confirmed by the presence of spots, as shown in Figure 4e. The spacing between the 0th-order (m = 0) and 1st-order (m = 1) spots corresponds to transmission diffraction angle of 1.504°. The diffraction data can be utilized to estimate the index change made within the modulating grating structure by the following equation[41,57–59]

$$m\lambda_{\text{incident}} = n_{\text{average}}\, d\sin\theta_{0-m} = \frac{n_{\text{low}} + n_{\text{high}}}{2}\, d\sin\theta_{0-m} \quad (1)$$

where m, $\lambda_{\text{incident}}$, n_{average}, d, θ_{0-m}, n_{low}, and n_{high} correspond to the diffraction order (= 1), the incident laser wavelength, the average index of the grating structure, the spacing (= 23.72 μm), the transmission diffraction angle of the 1st-order spot (= 1.504°), the refractive index of an unexposed region (= 3.175), and the refractive index of an exposed region, respectively. n_{high} of the exposed region is extracted to be 3.252, providing a refractive index change of 0.077 between the exposed and unexposed regions within the grating structure (i.e., $\Delta n = n_{\text{high}} - n_{\text{low}} = 3.252 - 3.175 = 0.077$). The index change closely matches the targeted Δn of 0.08. This confirms that the photothermal process-induced local increase in refractive index is evident, and more importantly, our novel process and material system exhibits definitive optical functionality in the form of an infrared diffraction grating. This finding points toward the feasibility of its use in other interrogated photonic applications where spatially controlled, index modulation is desired.

In summary, we have successfully demonstrated a novel photothermal process suitable for the manufacturing of low-cost, high precision microscale refractive and diffractive structures. By utilizing this approach to spatially modulate the concentration of sub-wavelength nanocrystals, we have demonstrated the ability to produce complex, arbitrary index gradients required for GRIN optics, with high spatial resolution. Radial index gradients which are fabricated within the GAP-Se glass have been shown to have unique dispersive properties not found in homogeneous media, such as ultralow dispersion across a broadband spectrum and negative Abbe numbers. This is the first ever material capable of achieving broadband achromatic performance using only a single optical element.

Experimental Section

Film Deposition and Stress Relieving Anneal: 0.134 μm thick $SiO_{0.9}$ AR coatings were deposited on fused silica substrates for 25 s at 300 °C, using 70 sccm of SiH_4 and 25 sccm of N_2O source gases with 2000 sccm of N_2 carrier gas at 300 W and 3.5×10^{-3} torr in the Applied Materials P-5000 plasma enhanced chemical vapor deposition chamber. Sequentially, 1.4 μm thick $14GeSe_2$–$42As_2Se_3$–44PbSe thin films were deposited by coevaporation of target materials for 10 min at room temperature, using 20 Å s^{-1} of $25GeSe_2$–$75As_2Se_3$ and 8.5 Å s^{-1} of PbSeat a growth pressure of 8×10^{-7} torr in the Kurt J. Lesker evaporator. Following the deposition processes, films underwent a stress-relieving anneal for 2 h at 145 °C under atmospheric pressure with N_2 carrier gas in the furnace CEE 4500.

Laser Exposure and Post-Thermal Treatment: A diode pumped Nd:$Y_3Al_5O_{12}$ (Nd:YAG) 1064 nm laser source (Lee Laser model LEP Y6TQ/30) was used for the laser exposure. The output laser beam was expanded to ≈10 mm diameter to over fill an 8 mm aperture. A series of laser dose exposures ranging from 1.26×10^2 to 1.51×10^4 J cm^{-2} were investigated. Following the laser exposure, the films were postannealed for 30–60 min at a variety of temperatures ranging from 150 to 200 °C on a temperature controlled hot plate.

Refractive Index Measurement: Refractive indices of the films were measured at wavelengths from 1.5 to 20 μm and angles from 69° to 75°, using J.A. Woollam IR–variable-angle spectroscopic ellipsometry (IR-VASE) including a Fourier transform infrared interferometer with a rotating compensator ellipsometer where IR light with a 8 mm beam spot is emitted by a Globar. Signals were collected by a deuterated triglycine sulfate detector.

Transmission Electron Microscopy Experiment: Cross-sectional specimens were prepared by ion milling followed by lift-out processing in the FEI Helios Nanolab 660 focused ion beam. The specimens were then mounted on Cu grids and ion-polished to ≈50 nm. TEM images, SAED patterns and XEDS data were collected in FEI Titan3 G2 TEMs operating at 200 keV.

Optical Simulation: The optical simulation was carried out using COMSOL Multiphysics software. The experimentally measured refractive indices of the layers including Au, GAP-Se film, AR coating, and fused silica substrate were used in the model. A plane wave with TE polarization was launched from the air side at the top boundary, and the other boundaries of the model were set with scattering boundary condition to mimic open boundaries.

Acknowledgements

This work was supported by the Defense Advanced Research Projects Agency under Air Force Research Laboratory contract FA8650-12-C-7225 through the M-GRIN Tech Area 2 program. The views, opinions, and/or

findings expressed are those of the author and should not be interpreted as representing the official views or policies of the Department of Defense or the U.S. Government (Distribution Statement "A": Approved for Public Release, Distribution Unlimited). The authors thank IRradiance Glass, Inc. for providing coefficient of thermal expansion-matched Class-4 glass substrates for film deposition.

Conflict of Interest

The authors declare no conflict of interest.

Keywords

achromatic microlenses, chalcogenide glass, gradient refractive index, optical nanocomposites, photothermal process

Received: June 8, 2018
Published online:

[1] D. T. Moore, *Appl. Opt.* **1980**, *19*, 1035.
[2] R. W. Wood, *Physical Optics*, MacMillan, **1905**.
[3] E. Hecht, *Optics*, Addison-Wesley, San Francisco, CA, USA **2001**.
[4] R. G. Driggers, *Encyclopedia of Optical Engineering*, Vol. *1*, CRC, New York **2003**.
[5] M. T. Flores-Arias, C. Bao, A. Castelo, M. V. Perez, C. Gomez-Reino, *Opt. Commun.* **2006**, *266*, 490.
[6] J. Teichman, J. Holzer, B. Balko, B. Fisher, L. Buckley, *Gradient Index Optics at DARPA*, The Institute for Defense Analyses, Alexandria, VA, USA **2014**.
[7] S. N. Houde-Walter, D. T. Moore, *Appl. Opt.* **1985**, *24*, 4326.
[8] S. Ji, M. Ponting, R. S. Lepkowicz, A. Rosenberg, R. Flynn, G. Beadie, E. Baer, *Opt. Express* **2012**, *20*, 26746.
[9] G. Beadie, J. S. Shirk, A. Rosenberg, P. A. Lane, E. Fleet, A. R. Kamdar, Y. Jin, M. Ponting, T. Kazmierzak, Y. Yang, A. Hiltner, E. Baer, *Opt. Express* **2008**, *16*, 11540.
[10] R. A. Flynn, E. F. Fleet, G. Beadie, J. S. Shirk, *Opt. Express* **2013**, *21*, 4970.
[11] D. Gibson, S. Bayya, V. Nguyen, J. Sanghera, M. Kotov, G. Drake, *Proc. SPIE* **2015**, *9451*, 94511P.
[12] F. Qiu, T. Narusawa, J. Zheng, *Appl. Opt.* **2011**, *50*, 733.
[13] F. Bociort, *J. Opt. Soc. Am. A* **1996**, *13*, 1277.
[14] P. K. Manhart, R. Blankenbecler, *Opt. Eng.* **1997**, *36*, 1607.
[15] L. Li, H. Lin, S. Qiao, Y. Zou, S. Danto, K. Richardson, J. D. Musgraves, N. Lu, J. Hu, *Nat. Photonics* **2014**, *8*, 643.
[16] H. Lin, L. Li, Y. Zou, S. Danto, J. D. Musgraves, K. Richardson, S. Kozacik, M. Murakowski, D. Prather, P. T. Lin, V. Singh, A. Agarwal, L. C. Kimerling, J. Hu, *Opt. Lett.* **2013**, *38*, 1470.
[17] P. T. Lin, V. Singh, J. Wang, H. Lin, J. Hu, K. Richardson, J. D. Musgraves, I. Luzinov, J. Hensley, L. C. Kimerling, A. Agarwal, *Opt. Mater. Express* **2013**, *3*, 1474.
[18] T. V. Galstian, J.-F. Viens, A. Villeneuve, M. A. Duguay, K. A. Richardson, *J. Lightwave Technol.* **1997**, *15*, 1343.
[19] A. Saliminia, K. L. Foulgoc, A. Villeneuve, T. Galstian, K. Richardson, *Fiber Integr. Opt.* **2001**, *20*, 151.
[20] K. Richardson, A. Buff, C. Smith, L. Sisken, J. David Musgraves, P. Wachtel, T. Mayer, A. Swisher, A. Pogrebnyakov, M. Kang, C. Pantano, D. Werner, A. Kirk, S. Aiken, C. Rivero-Baleine, *Proc. SPIE* **2016**, *9822*, 982205.
[21] J. Aizenberg, A. Tkachenko, S. Weiner, L. Addadi, G. Hendler, *Nature* **2001**, *412*, 819.
[22] M. J. Moghimi, J. Fernandes, A. Kanhere, H. Jiang, *Sci. Rep.* **2015**, *5*, 15861.
[23] E. A. Sanchez, M. Waldmann, C. B. Arnold, *Appl. Opt.* **2011**, *50*, 1974.
[24] P. Nussbaum, R. Volkel, H. P. Herzig, M. Eisner, S. Haselbeck, *Pure Appl. Opt.* **1997**, *6*, 617.
[25] B. A. Flusberg, E. D. Cocker, W. Piyawattanametha, J. C. Jung, E. L. M. Cheung, M. J. Schnitzer, *Nat. Methods* **2005**, *2*, 941.
[26] K. A. Arpin, A. Mihi, H. T. Johnson, A. J. Baca, J. A. Rogers, J. A. Lewis, P. V. Braun, *Adv. Mater.* **2010**, *22*, 1.
[27] G. Zuccarello, D. Scribner, R. Sands, L. J. Buckley, *Adv. Mater.* **2002**, *14*, 1261.
[28] A. Lepicard, F. Bondu, M. Kang, L. Sisken, A. Yadav, F. Adamietz, V. Rodriguez, K. Richardson, M. Dussauze, *Sci. Rep.* **2018**, *8*, 7388.
[29] B. J. Eggleton, B. Luther-Davies, K. Richardson, *Nat. Photonics* **2011**, *5*, 141.
[30] R. Frerichs, *J. Opt. Soc. Am.* **1953**, *43*, 1153.
[31] A. R. Hilton, *Chalcogenide Glasses for Infra-Red Optics*, McGraw Hill, New York **2010**.
[32] S. Parvanov, V. Vassilev, K. Tomova, *Mater. Lett.* **2008**, *62*, 2021.
[33] J. S. Sanghera, I. D. Aggarwal, *J. Non-Cryst. Solids* **1999**, *256–257*, 6.
[34] X. H. Zhang, H. Ma, J. Lucas, *Opt. Mater.* **2004**, *25*, 85.
[35] X. H. Zhang, Y. Guimond, Y. Bellec, *J. Non-Cryst. Solids* **2003**, *326–327*, 519.
[36] G. Yang, X. Zhang, J. Ren, Y. Yunxia, G. Chen, H. Ma, J. L. Adam, *J. Am. Ceram. Soc.* **2007**, *90*, 1500.
[37] H. Wang, X. Zhang, G. Yang, Y. Xu, H. Ma, J. L. Adam, Z. Gu, G. Chen, *Ceram. Int.* **2009**, *35*, 83.
[38] D. Zhao, F. Xia, G. Chen, X. Zhang, H. Ma, J. L. Adam, *J. Am. Ceram. Soc.* **2005**, *88*, 3143.
[39] F. Xia, X. Zhang, J. Ren, G. Chen, H. Ma, J. L. Adam, *J. Am. Ceram. Soc.* **2006**, *89*, 2154.
[40] L. Sisken, C. Smith, A. Buff, M. Kang, K. Chamma, P. Wachtel, J. D. Musgraves, C. Rivero-Baleine, A. Kirk, M. Kalinowski, M. Melvin, T. S. Mayer, K. Richardson, *Opt. Mater. Exp.* **2017**, *7*, 3077.
[41] L. Sisken, *Ph.D. Thesis*, University of Central Florida, Orlando, FL, USA **2017**.
[42] A. Buff, *Ph.D. Thesis*, University of Central Florida, Orlando, FL, USA **2016**.
[43] J. Lumeau, A. Sinitskii, L. Glebova, L. B. Glebov, E. D. Zanotto, *J. Non-Cryst. Solids* **2009**, *355*, 1760.
[44] T. Oikawa, T. Honma, T. Komatsu, *Cryst. Res. Technol.* **2008**, *43*, 1253.
[45] H. Zeng, Z. Liu, Q. Jiang, B. Li, C. Yang, Z. Shang, J. Ren, G. Chen, *J. Eur. Ceram. Soc.* **2014**, *34*, 4383.
[46] U. Kreibig, M. Vollmer, *Optical Properties of Metal Clusters*, Springer, Heidelberg, Germany **1995**.
[47] K. A. Richardson, J. M. McKinley, B. Joshi, S. Lawrence, A. Villeneuve, *Opt. Mater.* **1998**, *10*, 155.
[48] A. V. Belykh, O. M. Efimov, L. B. Glebov, Y. A. Matveev, A. M. Mekryukov, M. D. Mikhailov, K. A. Richardson, *J. Non-Cryst. Solids* **1997**, *213*, 330.
[49] K. Shimakawa, A. V. Kolobov, S. R. Elliott, *Adv. Phys.* **1995**, *44*, 475.
[50] P. Boolchand, *Insulating and Semiconducting Glasses*, World Scientific, Hackensack, NJ, USA **1999**.
[51] A. V. Kolobov, J. Tominaga, *Chalcogenide: Metastability and Phase Change Phenomena*, Springer, Heidelberg, Germany **2012**.
[52] C. T. Moynihan, P. B. Macedo, I. D. Aggarwal, U. E. Schnaus, *J. Non-Cryst. Solids* **1971**, *6*, 322.
[53] J. J. Mecholsky, G. R. Srinivasan, C. T. Moynihan, P. B. Macedo, *J. Non-Cryst. Solids* **1973**, *11*, 331.
[54] J. J. Mecholsky, C. T. Moynihan, P. B. Macedo, G. R. Srinivasan, *J. Mater. Sci.* **1976**, *11*, 1952.
[55] A. Yang, H. Lin, D. Chen, Y. Yu, Y. Wang, *Mater. Res. Bull.* **2014**, *49*, 193.
[56] A. Apling, A. J. Leadbetter, A. C. Wright, *J. Non-Cryst. Sol.* **1977**, *23*, 369.
[57] R. Collier, C. B. Buckart, L. H. Lin, *Optical Holography*, Academic, New York, **1971**.
[58] D. J. Cooke, L. Solymar, *J. Opt. Soc. Am.* **1980**, *70*, 1631.
[59] A. Heifetz, J. T. Shen, M. S. Shariar, *Am. J. Phys.* **2009**, *77*, 623.